State transition at electrohydrodynamic convection of twisted nematic liquid crystals

Chul Gyu Jhun,[1] Gyu Jin Choi,[2] Dae Geon Ryu,[2] Jong-Hoon Huh,[3,*] and Jin Seog Gwag[2,*]

[1]*School of Display Engineering, Hoseo University, Asan-shi, Chungnam 31499, Republic of Korea*

[2]*Department of Physics, Yeungnam University, 280 Daehak-Ro, Gyeongsan 38541, Republic of Korea*

[3]*Department of Mechanical Information Science and Technology, Faculty of Computer Science and Systems Engineering, Kyushu Institute of Technology, Iizuka, Fukuoka 820–8502, Japan*

(Received 6 August 2018; published 19 November 2018)

We study electrohydrodynamic convection (EHC) patterns in twisted nematic liquid crystal (TNCL) cells with an initial homeotropic alignment. In addition, we demonstrate switching characteristics due to the transition between the 90° and −90° twisted states. The pattern formations are similar to those obtained in a parallel-aligned nontwisted liquid crystal cell. Calculations of the free energy in an initially, homeotropically aligned TNLC in an electric field demonstrate that the energy barrier between the two states decreases with the increase of the electric field. The mutual transition is caused by the fluctuating flow at the dynamic scattering mode 2, where the energy barrier between the two states is reduced by applying a strong electric field. These properties may be employed for the development of a redirectable dynamic lenticular lens, as an extended version of the dynamic lenticular lens using EHC. The transition between the two states caused by EHC is reversible, and the convection roll pattern of the Williams domain rotates by 90° at each transition.

DOI: 10.1103/PhysRevE.98.052704

I. INTRODUCTION

Various nonlinear dissipative systems that exhibit pattern formations exist in nature, studied in scientific fields such as hydromechanics, atmosphere science, biology, chemistry, and so on [1,2]. Electrohydrodynamic convection (EHC) of a nematic liquid crystal (LC) is a representative example that exhibits a distinct pattern-forming phenomenon in fluid systems [3–17]. The patterns depend on the frequency, amplitude, and wave form of the electric field between two flat electrodes of a sandwiched LC cell. The fluctuating instabilities of the LC directors, as a function of the electric field, induce featured local space charges due to the anisotropic conductivity, which tend to destabilize the horizontally aligned LC state. The representative EHC pattern that emerges in the low-frequency conduction regime is a Williams domain, caused by the Carr-Helfrich instability [7]. The Williams domain can be observed by the optical focusing effect of the extraordinary ray parallel to the director, owing to the curvature of the undulated LC state with a small bending-type periodic distortion by a low-frequency electric field. The convection roll period of the Williams domain can be controlled by the cell thickness and electric field. The period and focal length decrease with an increase in the electric field, for a constant cell thickness. Therefore, it can act as a lenticular lens in a three-dimensional (3D) display. In addition, it can be used in two-dimensional-3D (2D-3D) switchable displays, as it can act as a two-dimensional (2D) display without a focusing effect in the absence of an electric field, and as a 3D display with a focusing effect due to EHC in the presence of an electric field.

Until now, EHC studies have mainly focused on the homogeneous LC alignment with a nontwisted state. There are few studies on the homeotropical LC alignment with a nontwisted state [18–22]. Twisted NLCs (TNLCs) with an initial homeotropic alignment have not been extensively investigated. The twisted structure of the LC cell is determined by surface-rubbed directions on the bottom and top substrates and the surface anchoring is an important factor that seriously affects the electrooptic characteristics of LC devices [23–33]. In general, it is not very likely that a 90° twisted state with an initially planar system transits into a −90° twisted state even under a convective flow by an electric field which leads to a director's fluctuations out of the plane, combined with an inhomogeneous charge distribution caused by the LC electric anisotropy. The director's deformation that causes an excessive bulk elastic energy in the presence of the applied vertical electric field is not large, as negative dielectric anisotropic LCs are employed. Therefore, the energy barrier between the two states is almost unchanged even if a strong electric field is applied. On the other hand, for the 90° twisted state with an initially, vertically aligned system, the bulk elastic energy caused by the significantly deformed director, in the presence of the strong electric field, is large, hence, the energy barrier is relatively low. Therefore, a transition between two states with EHC can occur more easily in a homeotropically aligned TNLC than in a horizontally aligned TNLC.

In this study, we examine EHC patterns in homeotropically aligned TNLC cells and demonstrate switching characteristics by the transition between the 90° and −90° twisted states. The mutual transition between the left-handed and right-handed twists by EHC, may be used in a reorientationable dynamic

*Corresponding authors: huh@mse.kyutech.ac.jp; sweat3000@ynu.ac.kr

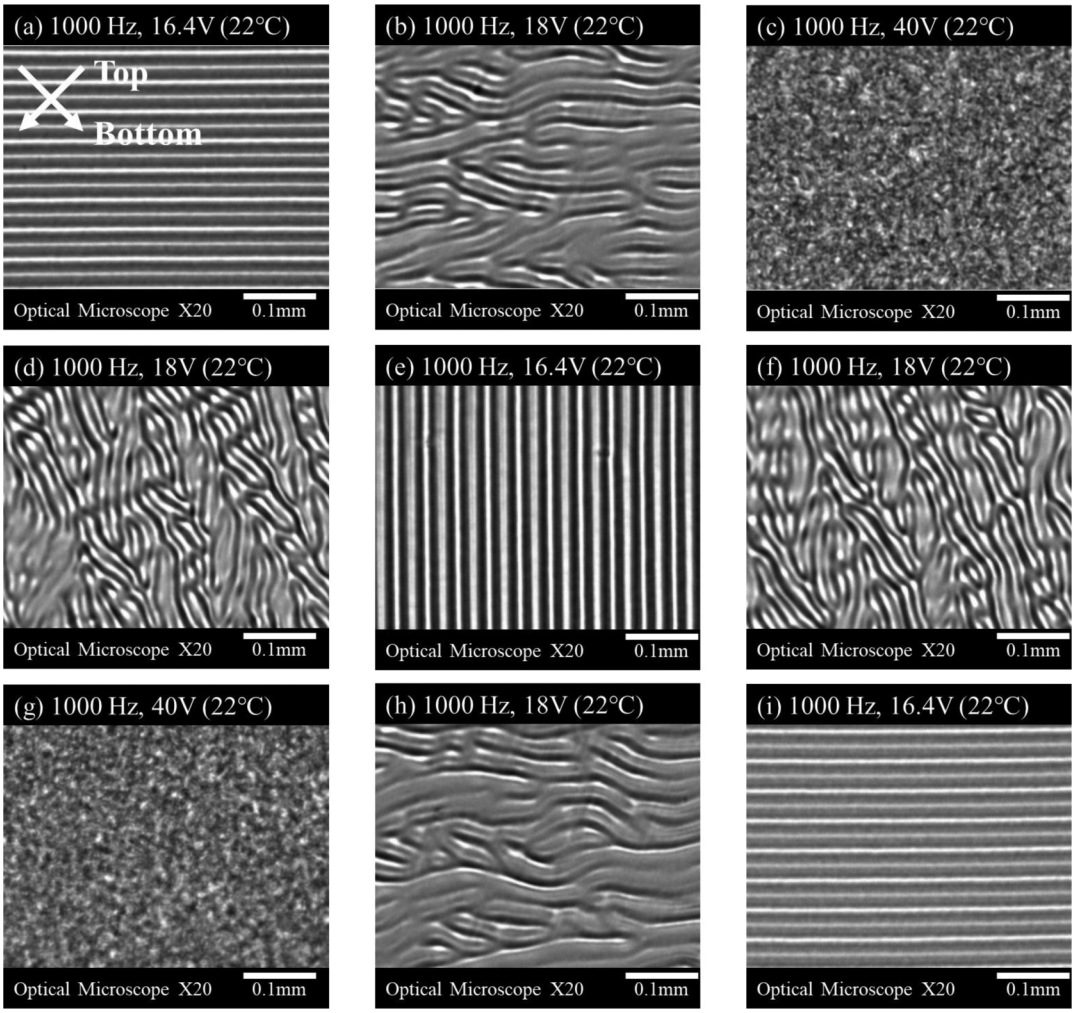

FIG. 1. Microscopic images of various EHC patterns according to frequency and applied voltage at homeotropic 90° TNLC cell. (a) Typical Williams domain, (b) a chevron pattern, (c) scattering mode, (d) a chevron pattern rotated by 90°, (e) William domain region rotated by 90°, (f) the chevron pattern rotated by 90°, (g) scattering mode, (h) a chevron pattern rotated by 90° again, and (i) Williams domain region rotated by 90° again.

lenticular lens, as an extended version of the dynamic lenticular lens using EHC.

II. EXPERIMENT

The LC material is an MBBA (*p*-methoxybenzylidene-*p*-*n*-butylaniline) which is LC with negative dielectric anisotropic; the elastic constants are $K_{11} = 6.66\,\text{pN}$, $K_{22} = 4.2\,\text{pN}$, and $K_{33} = 8.61\,\text{pN}$; the dielectric constants are $\varepsilon_{\parallel} = 4.72$ and $\varepsilon_{\perp} = 5.25$. The ratio of cell thickness to pitch is $d/p = 0.25$; the pretilt angle is 85°; the cell thickness is 10 μm. A polyimide (SE-1211 provided by Nissan Chemical) as a homeotropic LC alignment layer is used. The liquid crystal material without any chiral dopant was injected into a empty cell assembled after rubbing the polyimide spin-coated on indium-tin-oxide (ITO) films deposited by using a RF magnetron sputtering system on two glass substrates ($3 \times 3\,\text{cm}^2$). The homeotropic polyimide was spin-coated in two steps, 1000 rpm for 10 s and 3500 rpm for 20 s, to produce an initially vertically aligned LCs and the heat treatment progressed in two steps, 100 °C for 30 minutes and 250 °C for 1 hour and 30 minutes. The thickness of the cell was fixed at about 10 μm by using glass beads. To make the 90° twisted LC state under a vertical electric field, we rubbed the bottom and top substrates to −45° and −135° directions by a velvet-type rubbing machine, respectively. The rubbing conditions are as follows; the rotation speed of the roll, the rubbing depth, and the speed of the rubbing stage are 900 rpm, 3 mm, and 2 cm/s, respectively. Then, the pretilt angle of LDs was distributed within 85–88°. EHC patterns at fabricated LC cells were observed under 22 °C and the frequency of 1000 Hz of the conduction region.

III. RESULTS

Figure 1 shows microscopic images of various EHC patterns as a function of the frequency and applied voltage in a homeotropic 90° TNLC cell. A typical Williams domain emerges at the low-frequency and low-voltage conduction region, as shown in Fig. 1(a). In Fig. 1(a), the top and bottom substrates are denoted as T and B, and the arrows represent the rubbing directions at −45° and −135°, with respect to

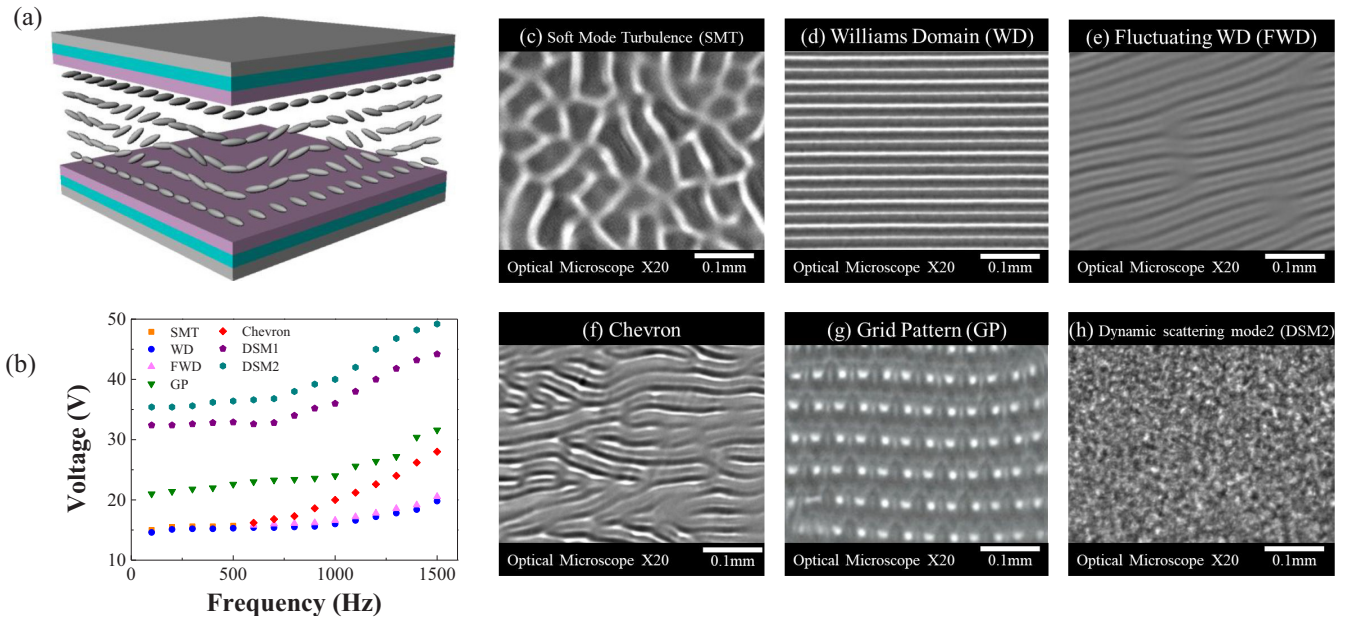

FIG. 2. Schematic, EHC mode diagram, and the microscopic images of EHC patterns of 90° twisted state. (a) Schematic of 90° twisted state with EHC, (b) bifurcation diagram of 90° twisted state with EHC, (c) soft mode turbulence (SMT) observed at 500 Hz and 15.5 V, (d) Williams domain (WD) observed at 1000 Hz and 16.4 V, (e) the fluctuating Williams domain (FWD) observed at 1000 Hz and 17 V, (g) chevron pattern observed at 1000 Hz and 18 V, (f) grid pattern (GP) observed at 1000 Hz and 24 V, and (h) dynamic scattering mode2 (DSM2) observed at 1000 Hz and 40 V.

the direction of the EHC (azimuthal, 0°). Figure 1(a) shows that a typical Williams domain appears at the low frequency (1000 Hz) and low voltage (16.4 V) region. The EHC flows along the midplane director of the twisted LC layer [17]. A chevron pattern is observed in the same frequency (1000 Hz) and voltage (18 V) dielectric region, as shown in Fig. 1(b). For a fixed frequency, a dynamic scattering mode2 (DSM2) appears when the voltage is slightly increased (40 V), as shown in Fig. 1(c). When the voltage is decreased to the lower value of 18 V, EHC occurs and a chevron pattern appears; however, the direction of the pattern is rotated by 90°, as shown in Fig. 1(d). The rotation of the pattern can be clearly observed when the voltage is reduced to a value in the Williams domain region (1000 Hz and 16.4 V), as shown in Fig. 1(e). We can notice that the roll direction is completely rotated by 90°. This rotation is caused by the state transition from the 90° twisted state to the −90° twisted state in the TNLC cell. The driving force of the state transition is the electric field and chaotic scattering mode. The energy barrier between the two LC states is lowered by the electric field, and the strong scattering state at which the LCs fluctuate moves a twisted LC state over the lowered barrier to another twisted LC state. To examine whether the scattering mode generates the state transition, we increased the voltage to reach the scattering pattern [Fig. 1(g)] through the chevron region [Fig. 1(f)] at the −90° twisted state, and then decreased it to values of the Williams domain region [Fig. 1(i)] through the chevron pattern [Fig. 1(h)]. We confirm that the scattering state (DSM2) generates a state transition, as Figs. 1(f) to 1(i) show that the direction of the roll pattern is rotated again by 90° after passing through the DSM2.

For a detailed analysis of these results, we observed the EHC mode diagram for the 90° and −90° twisted states. Figure 2(a) illustrates the 90° twisted state with EHC. Figure 2(b) shows the bifurcation diagram for the 90° twisted state with EHC. Significantly different regimes are observed below and above the threshold voltage and frequency; these results are very similar to those of a nontwisted LC cell. Our experiment was performed only at conduction region with low frequency and voltage. For conduction region [$f < f_c$, (f_c: threshold frequency)], we observe Williams domains with a spatial periodicity that depends on the thickness (d) of the LC cell. The threshold value as a function of the frequency can be expressed, for a nontwisted LC cell, as $V_c = V_0^2(1+\omega^2\tau^2)/(\upsilon^2 - 1 - \omega^2\tau^2)$, where $V_0 = [-4\pi^3\varepsilon_{ll}/(\varepsilon_{ll} - \varepsilon_\perp)\varepsilon_\perp K_{22}]^{1/2}$, while τ and υ are the dielectric charge relaxation time and dimensionless coefficient, respectively [34]. Figures 2(c) to 2(h) show microscopic images of the EHC pattern modes as a function of the frequency and voltage of the 90° twisted state. The typical patterns of a conventional parallel and antiparallel aligned LC cell are observed. Soft-mode turbulence (SMT) with a nonlinear pattern appears at low frequencies and voltages below 500 Hz and 20 V, respectively, in the conduction regime, as shown in Fig. 2(c). It corresponds to a slowly varying azimuthal rotation of the LCs and can easily couple to the EHC modes. The Williams domain emerges when the frequency and voltage are slightly increased from the edge of the SMT, as shown in Fig. 2(d). A fluctuating Williams domain appears with the increase of the voltage from the Williams domain, as shown in Fig. 2(e). Higher voltages lead to a grid pattern (GP), one of the complex patterns of the conduction regime, as shown in Fig. 2(f). At the higher voltage, a chevron pattern appears, as shown in Fig. 2(g). Higher voltages generate a dynamic scattering mode2 (DSM2) that has a strongly nonlinear-chaotic pattern, as shown in Fig. 2(h). In addition, we observed an

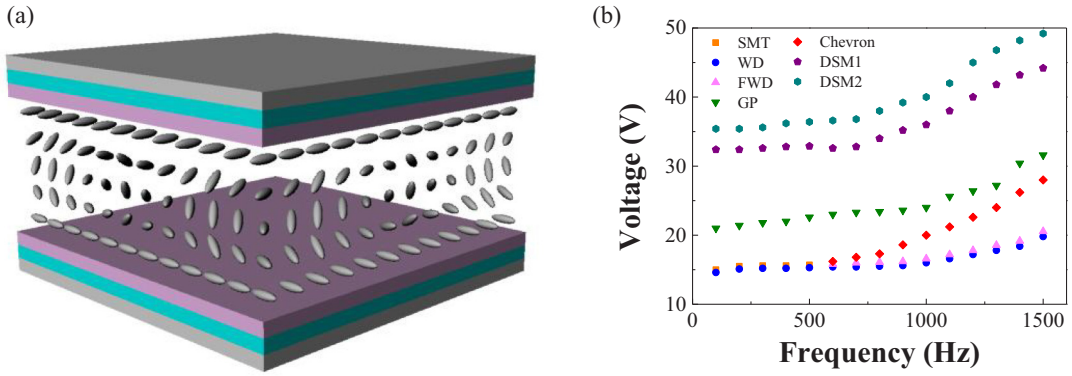

FIG. 3. Schematic and EHC mode diagram of EHC patterns of −90° twisted state. (a) Schematic of −90° twisted state with EHC and (b) bifurcation diagram of −90° twisted state with EHC.

EHC pattern diagram after the transition from a 90° to a −90° twisted state. It is similar to the diagram of the 90° twisted state, as shown in Fig. 3, even though there is a slight difference in frequency and voltage. This may imply that the EHC patterns are determined by the initial parameters of the LC cell, such as the cell thickness, absolute value of the twisted angle, pretilt angle, and elastic constants that contribute to the change of the free energy as a function of the frequency and voltage.

IV. THEORETICAL ANALYSIS

To describe the bistability (left- and right-handed twists) in the presence of the electric field in a 90° TNLC cell using a homeotropic alignment layer (SE-1211 provided from Nissan Chem. Co.), we calculated the free energy by considering the electric fields at each twisted angle. The free energy density is [35]

$$F = \int_0^d \left[\frac{f(\theta)}{2}\left(\frac{\partial\theta}{\partial z}\right)^2 + \frac{g(\theta)}{2}\left(\frac{\partial\phi}{\partial z}\right)^2 + e(\theta)\left(\frac{\partial\phi}{\partial z}\right) + \frac{K_{22}q_0^2}{2}\right] dz + F_s + F_e, \quad (1)$$

where

$$f(\theta) = K_{11}\sin^2\theta + K_{33}\cos^2\theta, \quad (2)$$

$$g(\theta) = (K_{22}\sin^2\theta + K_{33}\cos^2\theta)\sin^2\theta, \quad (3)$$

$$e(\theta) = -2q_0K_{22}\sin^2\theta. \quad (4)$$

where θ and ϕ are the polar and azimuthal angles of the LC directors, respectively; K_{11}, K_{22}, and K_{33} are the splay, twist, and bend elastic constants of the LC material, respectively; and q_0 is the chirality that is related to the pitch P_0 by $q_0 = 2\pi/P_0$. However, it is zero for our experiment because any chiral material was not added into LC. The surface anchoring energy F_s is obtained using the Rapini-Papoular surface potential [36]

$$F_s = \tfrac{1}{2}A_p\sin^2(\theta-\theta_0) + \tfrac{1}{2}A_a\sin^2(\phi-\phi_0), \quad (5)$$

where A_p and A_a are the polar and azimuthal anchoring coefficients, respectively. The electric energy F_e of the electric field is

$$F_e = -\tfrac{1}{2}\varepsilon_0\varepsilon_\perp\vec{E}^2 - \tfrac{1}{2}\varepsilon_0\Delta\varepsilon(\vec{n}\cdot\vec{E})^2. \quad (6)$$

To obtain a bistable feature in the presence of an electric field for the homeotropic 90° TNLC cell, we used Eqs. (1) to (6). We revealed the variations of the Gibbs free energy

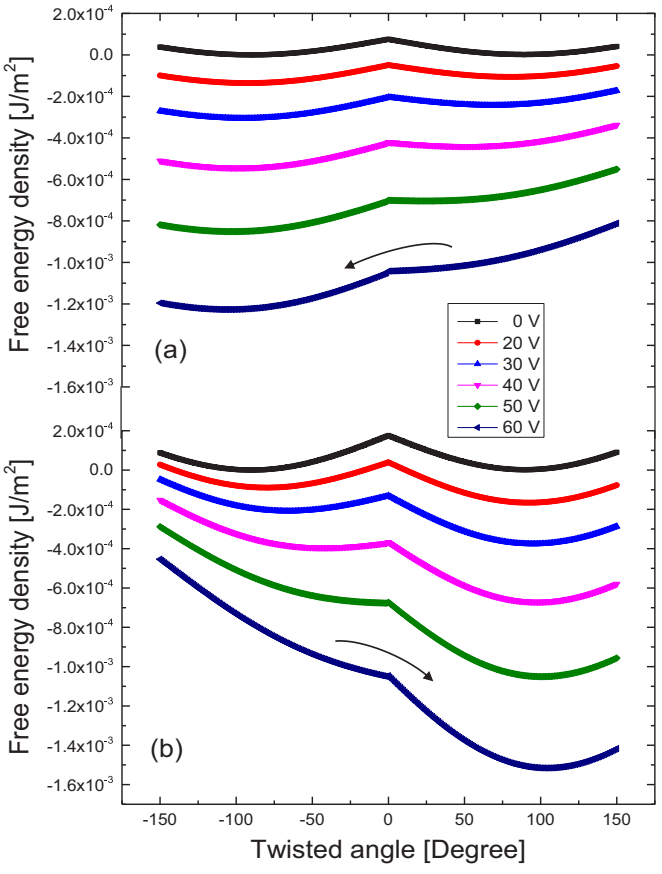

FIG. 4. The change of bistable curve according to the strength of the fields at TNLC cell with orthogonally rubbed two surface boundaries. (a) Free energy density at 90° twisted state and (b) free energy density of −90° twisted state.

density as a function of the twist angle for various fields at the TNLC cell using straightforward calculations [37,38].

We assume that the twisted angles of the LC directors vary linearly throughout the cell. The LC director at the bottom is along the x axis, while that at the top substrate is along the y axis. The LC directors initially have a 90° right-handed twist. The following parameters were used in the numerical calculations. The LC material is an MBBA (p-methoxybenzylidene-p-n-butylaniline), which is LC with negative dielectric anisotropy; the elastic constants are $K_{11} = 6.66\,\text{pN}$, $K_{22} = 4.2\,\text{pN}$, and $K_{33} = 8.61\,\text{pN}$; $\varepsilon_{\parallel} = 4.72$ and $\varepsilon_{\perp} = 5.25$; $d/p = 0.25$; the pretilt angle is 85°; the cell thickness is 10 μm. The polar and azimuthal anchoring coefficients are set to $1 \times 10^{-5}\,\text{J/m}^2$ and $1 \times 10^{-6}\,\text{J/m}^2$, respectively, and the anchoring energy for the top and bottom substrates is assumed to be symmetrical. Taking into account the horizontal electric field caused by the local space charges, the electric field was applied azimuthally, along the 45° direction for the 90° twisted state and along the −45° for the −90° twisted state, as the charge accumulation direction is perpendicular to the direction of the EHC that flows along the midplane director of the twisted LC layer [17]. Therefore, the electric field is tilted with respect to the vertical direction.

The changes of the bistable curve as a function of the strength of the field at the TNLC cell with two orthogonal rubbed surface boundaries are shown in Fig. 4. For an initial 90° twisted state without an applied electric field, the 90° and −90° twisted states are identically stable, i.e., they correspond to the minimum of the free energy. With the increase of the horizontal electric field tilted along the azimuthal 45° direction, the energy barrier from the 90° twisted state to the −90° twisted state gradually decreases, as shown in Fig. 4(a). For large values of the applied voltage, the bistable becomes almost a monostable configuration. In such a case, a transition to −90° twisted state can easily occur through the complex convection flow of the scattering mode that fluctuates the free energy. For the −90° twisted state after the transition, the EHC direction is rotated by 90°, hence a convection roll along the −45° direction emerges at the Williams domain. Subsequently, the vertically applied electric field is slightly tilted towards the azimuthal −45° direction, as the accumulated electrical charge direction reaches the azimuthal −45° direction. With the increase of the vertical electric field tilted towards the azimuthal −45° direction, the energy barrier from the −90° twisted state to the 90° twisted state gradually decreases, as illustrated in Fig. 4(b). The transition to the 90° twisted state can easily occur through the complex convection flow of the scattering mode that fluctuates the free energy. The simulation results show that the transition from the −90° twisted state to the 90° twisted state is strongly dependent on the electric field strength. If the electric field strength is larger than the critical value at which the energy barrier almost disappears between the 90° and −90° twisted states, a transition to the counter state can occur; they become easily switchable. Even though the free-energy theory may not be enough to explain this state transition in a dissipative system, it can be seen that the experimental result is analyzed satisfactorily up to a point. In the future, it is expected that other researchers will be able to explain this result better if further calculations are performed using other major factors.

V. SWITCHING OF STATES

The images in Fig. 5 show that the two states that have mutually orthogonal convection roll patterns are switched when a voltage that has a proper frequency is applied to the top and bottom electrodes that generate the vertical electric field. The transition time is approximately 3 s for an applied voltage of 16.4 V with a frequency of 1000 Hz, after the application of a rectangular waveform that has a voltage of

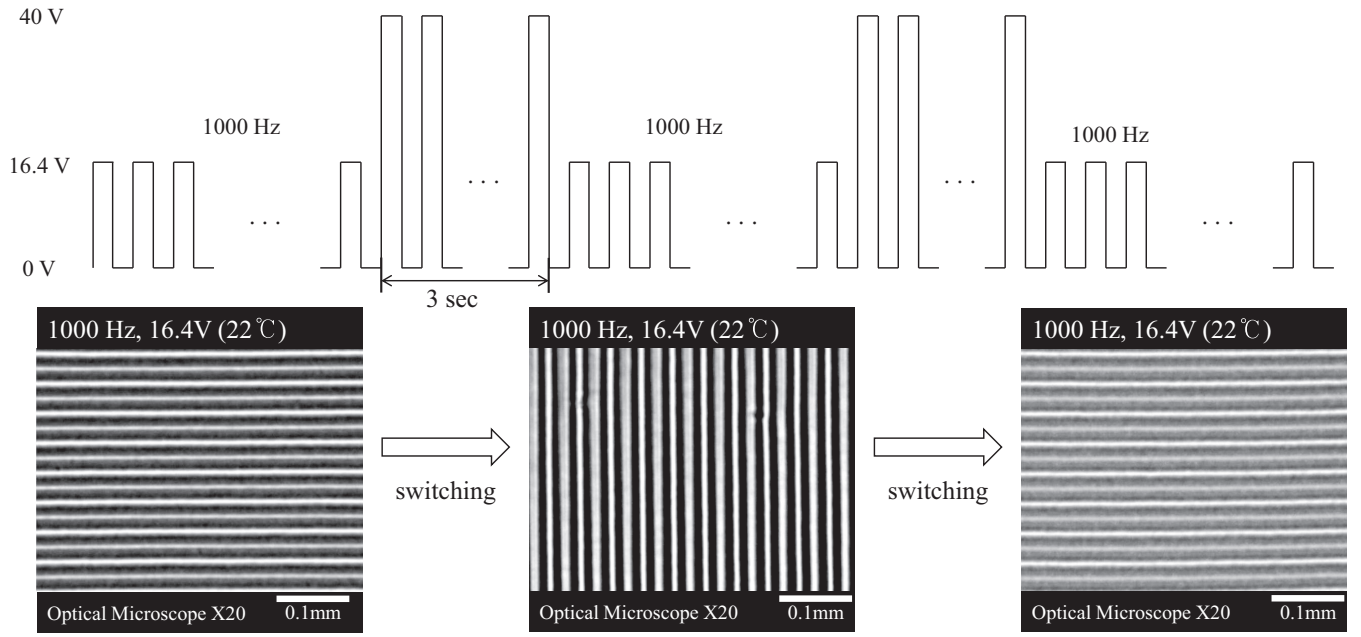

FIG. 5. Images showing that the two states of which convection roll patterns are mutually orthogonal are switched when voltage with a proper frequency is applied to the top and bottom electrodes that generate vertical electric field.

40 V and a frequency of 1000 Hz for 3 s. The results showed that the transition was reversible; hence it was continuously switching during the performed tests. Therefore, the mutual state transition between the two states with EHC may be employed for a reorientationable dynamic lenticular lens, as an extended version of the dynamic lenticular lens using EHC.

VI. CONCLUSION

In conclusion, we examine the EHC patterns in a homeotropically aligned TNLC cell. The pattern formations are similar to those obtained in a parallel-aligned nontwisted LC cell. We demonstrate switching characteristics of the transition between the 90° and −90° twisted states. The calculations of the free energy of the TNLC cell show that the transition between the two states with EHC can occur more easily in a homeotropically aligned TNLC, compared to a horizontally aligned TNLC. The mutual transition is caused by the fluctuating flow at the DSM2, where the energy barrier between the two states is reduced using a strong electric field. These properties may be applied for the development of a redirectable dynamic lenticular lens, as an extended version of the dynamic lenticular lens using EHC, as the transition between the two states by EHC is reversible, and the roll pattern rotates by 90° at each transition.

ACKNOWLEGMENT

This work was supported through the Basic Science Research Program through the National Research Foundation of Korea (NRF) funded by the Ministry of Science, ICT, and Future Planning (Grant No. 2016R1D1A3B03932396).

[1] W. Horsthemke and R. Lefever, *Noise-Induced Transition* (Springer, Berlin, 1984).
[2] J. Garcia-Ojalvo and J. M. Sancho, *Noise in Spatially Extended Systems* (Springer, New York, 1999).
[3] R. Williams, J. Chem. Phys. **39**, 384 (1963).
[4] E. F. Carr, Mol. Cryst. **7**, 253 (1969).
[5] L. Kramer and W. Pesch, Annu. Rev. Fluid Mech. **27**, 515 (1995).
[6] S. Kai and W. Zimmermann, Prog. Theor. Phys. Suppl. **99**, 458 (1989).
[7] W. Helfrich, J. Chem. Phys. **51**, 4092 (1969).
[8] M. C. Cross and P. C. Hohenberg, Rev. Mod. Phys. **65**, 851 (1993).
[9] T. Toth-Katona and J. T. Gleeson, Phys. Rev. E **69**, 016302 (2004).
[10] J. T. Gleeson, Phys. Rev. E **63**, 026306 (2001).
[11] P. Coullet, L. Gil, and J. Lega, Phys. Rev. Lett. **62**, 1619 (1989).
[12] G. Goren, I. Procaccia, S. Rasenat, and V. Steinberg, Phys. Rev. Lett. **63**, 1237 (1989).
[13] T. Toth-Katona, N. Eber, and A. Buka, Phys. Rev. E **83**, 061704 (2011).
[14] J.-H. Huh, Phys. Rev. E **92**, 062504 (2015).
[15] J.-H. Huh, Y. Hidaka, A. G. Rossberg, and S. Kai, Phys. Rev. E **61**, 2769 (2000).
[16] J.-H. Huh, Y. Yusuf, Y. Hidaka, and S. Kai, Phys. Rev. E **66**, 031705 (2002).
[17] G. J. Choi, J. M. Song, C. G. Jhun, J.-H. Huh, and J. S. Gwag, Phys. Rev. E **96**, 040701 (2017).
[18] A. Hertrich, W. Decker, W. Pesch, and L. Kramer, J. Phys. II France **2**, 1915 (1992).
[19] H. Richter, A. Buka, and I. Rehberg, Mol. Cryst. Liq. Cryst. **251**, 181 (1994); Phys. Rev. E **51**, 5886 (1995).
[20] A. G. Rossberg, A. Hertrich, L. Kramer, and W. Pesch, Phys. Rev. Lett. **76**, 4729 (1996).
[21] S. Kai, K. Hayashi, and Y. Hidaka, J. Phys. Chem. **100**, 19007 (1996).
[22] Y. Hidaka, J.-H. Huh, K.-I. Hayashi, S. Kai, and M. I. Tribelsky, Phys. Rev. E **56**, R6256(R) (1997); Y. Hidaka, J.-H. Huh, K. Hayashi, M. I. Tribelsky, and S. Kai, J. Phys. Soc. Jpn. **66**, 3329 (1997).
[23] D. W. Berreman, Phys. Rev. Lett. **28**, 1683 (1972).
[24] S. Faetti and P. Marianelli, Phys. Rev. E **72**, 051708 (2005).
[25] J. S. Gwag, J. Fukuda, M. Yoneya, and H. Yokoyama, Appl. Phys. Lett. **91**, 073504 (2007).
[26] J. S. Gwag, J. H. Kwon, M. Oh-e, J. Niitsuma, M. Yoneya, and H. Yokoyama, Appl. Phys. Lett. **95**, 103101 (2009).
[27] H. Yokoyama and H. A. van Sprang, J. Appl. Phys. **57**, 4520 (1985).
[28] T. Araki, M. Buscaglia, T. Bellini, and H. Tanaka, Nat. Mater. **10**, 303 (2011).
[29] J. I. Fukuda, M. Yoneya, and H. Yokoyama, Phys. Rev. Lett. **98**, 187803 (2007).
[30] G. P. Bryan-Brown, E. L. Wood, and I. C. Sage, Nature **399**, 338 (1999).
[31] G. J. Choi, Q. V. Le, K. S. Choi, K. C. K, H. W. Jang, J. S. Gwag, and S. Y. Kim, Adv. Matter. **29**, 1702598 (2017).
[32] J. S. Gwag, S. J. Kim, J. G. You, J. Y. Lee, J. C. Kim, and T.-H. Yoon, Opt. Lett. **30**, 1387 (2005).
[33] J. H. Kim, M. Yoneya, and H. Yokoyama, Nature **420**, 159 (2002).
[34] E. Dubois-Violette, P. G. de Gennes, and O. Parodi, J. Phys. (France) **32**, 305 (1971).
[35] P. G. de Gennes and J. Prost, *The Physics of Liquid Crystals* (Clarendon, Oxford, 1993).
[36] A. Papini and M. Papoular, J. Phys. (Paris) Colloq. **30**C4 (1969).
[37] S. Saito, T. Takahashi, T. Chiba, and S. Tsuchida, Jpn. J. Appl. Phys. **41**, 3841 (2002).
[38] C. G. Jhun, C. P. Chen, S. L. Lee, J. I. Back, T.-H. Yoon, and J. C. Kim, Jpn. J. Appl. Phys. **45**, 5063 (2006).